Exp Fluids (2006) 41:629–640
DOI 10.1007/s00348-006-0186-x

RESEARCH ARTICLE

Measurement of the gradient field of a turbulent free surface

Ralph Savelsberg · Ad Holten · Willem van de Water

Received: 6 April 2006 / Revised: 13 June 2006 / Accepted: 27 June 2006 / Published online: 19 August 2006

Abstract We study the free surface above a turbulent channel flow. We describe a laser scanning technique that can be used to measure the space–time turbulent surface gradient field along a line. A harmonically swiveling laser beam is focused on the surface and its angle of refraction is measured using a position sensing device. The registered signals can be converted easily to the desired gradient field, and spectra and correlations can be measured. Examples of measured spectra and correlation functions of the surface above a turbulent channel flow (Reynolds number $R_\lambda \approx 250$) demonstrate the viability of the technique. We further assess the validity of Taylor's frozen turbulence hypothesis that implies that time-dependent signals measured along a line that is oriented perpendicularly to the mean channel velocity can be interpreted as 2D measurements of the surface slope. While Taylor's hypothesis works for a turbulent velocity field, it does not work for its free surface.

PACS 47.27.-i · 47.27.Gs · 47.55.N-

1 Introduction

The small-scale roughness of the ocean's surface determines the exchange of heat and mass between the atmosphere and the ocean. These transport processes are crucial for the global distribution of momentum, heat and chemical species. In a geophysical setting, the ocean surface is wrinkled by the wind and the turbulent motion of the flow beneath it. In our work, we concentrate on the wrinkling of the free surface on a turbulent flow in still air. A central question is the relation between the statistical properties of the surface and those of the bulk turbulence beneath it. For example, whether there exists a simple relation between the spectrum of the surface elevation and that of the velocity field.

The problem is that no known precise and linear devices exist that can measure the surface in space and time. As the spectral energy $E(k)$ of the surface elevation decreases rapidly with increasing wave number, it is desirable to measure the surface slope rather than its height, as the former decreases much more slowly as $k^2\,E(k)$.

One of the first quantitative measurements of the surface gradient field involved pictures of the sun glittering on the ocean surface (Cox and Munk 1954). In our work we use the refraction of a focused laser beam by the surface to measure the two components of the surface gradient in a point. By rapidly scanning the incident laser beam along a line, while at the same time sampling the location of the refracted laser beam, we measure the time-dependent gradient field along a line. For strongly curved surfaces, scanning techniques are unavoidable because whole-field measurements are thwarted by caustics and ambiguities. A similar scanning slope gauge has been described by Bock and Hara (1995) and Hara et al. (1997). Their device, which was successfully used for the measurement of wind-driven waves, is suited for relatively low frequencies and large wavelengths (largest frequency ≈ 35 Hz, smallest wavelength ≈ 4 mm) and scans a circle on the surface. For our experiment a linear scan and a much better space–time resolution was needed.

R. Savelsberg · A. Holten · W. van de Water (✉)
Physics Department, Eindhoven University of Technology,
P.O. Box 513, 5600 MB Eindhoven, The Netherlands
e-mail: w.v.d.water@tue.nl

Jähne et al. (1994) review quantitative imaging techniques of ocean wind waves and conclude that scanning techniques for measuring the gradient field are most promising. It is good however, to put these techniques in the perspective of whole field measurements. In this context, an often-used technique to look at spatial surface deformations is shadowgraphy (Settles 2001). In shadowgraphy, images are formed as a result of the refraction of light passing through a transparent material of varying density. In the case of a free surface this refraction occurs at the interface and the resulting image provides a view of the shape of the surface. For free-surface flows, shadowgraphy has mainly been used to study the interaction of structures with the surface. For instance, Walker et al. (1995) have used shadowgraphy to study the interaction between a turbulent jet and a free surface. Sarpkaya and Suthon (1991), Gharib (1994) and Gharib and Weigand (1996) have used shadowgraphy to study vortex (dis)connection and the interaction between vortex rings and a free surface. Studying this same problem, Weigand (1996) has combined shadowgraphy with PIV to obtain information on the link between the free surface shape and the subsurface velocity field. However, obtaining quantitative information from shadowgraphy is often impossible and shadowgraphy is primarily a tool to qualitatively visualize the surface shape.

Zhang and Cox (1994) and Kurata et al. (1990) show that quantitative information about the surface gradient field can be obtained from images of a (colored) pattern that is either refracted in or reflected by the surface. By reducing the scale of these patterns, Dalziel et al. (2000) propose a synthetic schlieren technique in which a randomly dotted pattern is refracted by the free surface. Quantitative information about the surface shape is obtained by applying a cross-correlation algorithm, similar to that used for particle image velocimetry (PIV), to a picture of the undisturbed pattern and a picture of the refracted pattern. All of these techniques are image-based. The actual image itself provides the (2D) spatial information. The spatial resolution of these techniques is limited by the density of the pattern used, or in case of the synthetic schlieren technique by the minimum size of the interrogation windows used for cross-correlating the images. The resolution in time in these techniques is limited by the frame-rate of the camera. Increasing the frame-rate, through the use of a high-speed camera, has consequences for the measurement of low frequencies, since the duration of the measurement is limited by the maximum number of frames that can be stored.

In a geophysical setting, on an entirely different scale both in space (from several meters up to kilometers) and in time (frequencies lower than 1 Hz), several different techniques are used to measure wave-fields, including radar (altimeter) measurements from ships (Senet et al. 2001) or even from satellites (Forbes et al. 1993; Stammer 1997) and photographs of sea surface glint taken from aircraft (Dugan and Piotrowski 2003), as well as measurements from in situ arrays of buoys and pressure transducers (Holland 2001).

In this paper, we will describe a laser scanning device that has allowed us to answer a few basic questions about the relation between the surface gradient field and the turbulent velocity field beneath it. Details about these answers will be given elsewhere; in this paper we will concentrate on the measurement technique. First we will describe the experimental setup, the surface scanner, the timing electronics and the software used to extract the space–time gradient field from the measured signals. It will turn out that calibration of this device needs the measurement of only three geometrical factors. Next we will discuss the statistical quantities which are of interest in the context of this study, and provide results. These results show the viability of our method and reveal where it could be further improved.

We measure the time-dependent gradient field along a line which is oriented perpendicularly to the mean velocity of the free surface of a turbulent channel flow. An interesting question is whether Taylor's frozen turbulence hypothesis can be invoked in this context, that is whether the space–time measurement of the surface gradient can be viewed as a 2D *spatial* scan of the gradient field.

2 Experimental setup

We measure the gradient field of a free surface on a turbulent channel flow. The experimental setup is sketched in Fig. 1. Relatively strong turbulence is generated in a water channel (cross-section 0.3×0.4 m^2) by means of an active grid. At the measurement location (2 m downstream from the grid) the turbulence is isotropic with Taylor-based Reynolds number $R_\lambda \approx 250$ and mean velocity $U = 0.25$ m/s. This results in energy spectra in which an inertial range can be clearly recognized. Weaker turbulence with $R_\lambda \approx 70$ was generated using a simple stationary grid. The turbulence beneath the free surface was characterized using laser–Doppler anemometry and PIV. A challenge in this experiment is the simultaneous measurement of the surface gradient field and the 2D projection of the velocity field in a plane just below the surface.

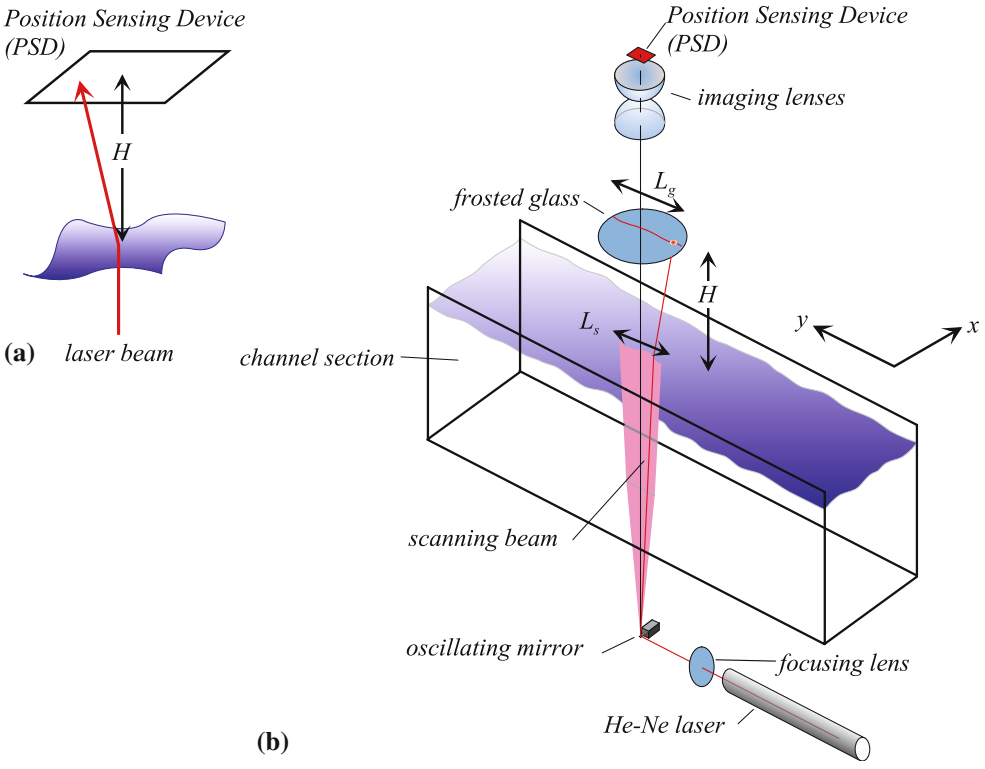

Fig. 1 **a** Principle of surface gradient measurement through refraction of a laser beam through the surface. The coordinates of the laser beam are measured using a position sensing device. Its average height above the surface is H. **b** Experimental setup. We measure the slope of the free surface of a turbulent channel flow. A laser beam is focused onto the surface, and is scanned (scanning frequency 2 kHz) along a line (length L_s) on the surface using an oscillating mirror. The refracted laser beam hits a translucent screen, and the laser spot is imaged onto a position sensing device using two strong lenses. The conversion of the registered PSD signals to the time-dependent surface gradient along a line only needs the geometrical quantities L_s, H, and L_g

In this paper, we will discuss the technique of the surface gradient measurement. This is done most naturally by first describing the measurement of the surface slope in a point, and next extending this to a line measurement.

2.1 Point measurement of the surface gradient

The principle of the technique used to do point measurements of the slope is based on refraction of a laser beam. The method was successfully used by us to measure waves on the surface of a vertically oscillated fluid (Faraday waves) (Westra et al. 2003).

A laser beam is sent perpendicularly through the transparent bottom of the water-channel and onwards to the surface, where it is refracted. The refracted beam then proceeds onto a so-called position sensitive device (PSD) (Fig. 1a). This sensor (manufactured by UDT corp.) is a dual lateral photo-diode, with a surface area of 2×2 cm^2. After being given a voltage bias, the sensor produces four photo currents, whose ratios determine a location of the laser spot on the sensor surface. Because of these ratios, the sensor is insensitive to the intensity of the laser spot, with the position signal reflecting the center of mass of the laser spot. We emphasize that this only works if the four photo-currents can be measured exactly simultaneously and the transport of the photo charges across the sensor is instantaneous. The four photo-currents were sampled with 12 bits precision at 300 kHz and the divisions needed for computation of the laser spot coordinates x_{PSD} and y_{PSD} were done in software. Generally, a PSD offers a far better resolution in time than a pixel-based detector such as a CCD or CMOS. The spatial resolution of the PSD is limited by both shot noise and thermal noise of the resistive layer. The linearity of the response is primarily dependent on the quality of the substrate layers of the PSD. In practice, we use a linear transformation from voltages to positions, based on a separate calibration of the PSD.

The free surface gradient in x and y-directions can be calculated from the displacements δx, δy of the spot on the PSD surface from:

$$\frac{\partial h}{\partial x} = \frac{\delta x}{n_w \sqrt{H^2 + (\delta x)^2 + (\delta y)^2} - H} \quad \text{and}$$

$$\frac{\partial h}{\partial y} = \frac{\delta y}{n_w \sqrt{H^2 + (\delta x)^2 + (\delta y)^2} - H},$$

where H is the height of the PSD above the undisturbed surface, and n_{w} is the refractive index of water. The displacements δx, δy are calculated by subtracting the average position of the spot taken over the entire measurement time from the instantaneous position,

$$\delta x = x_{\mathrm{PSD}} - \langle x_{\mathrm{PSD}} \rangle,\ \delta y = y_{\mathrm{PSD}} - \langle y_{\mathrm{PSD}} \rangle, \quad (2)$$

where x_{PSD} and y_{PSD} are the instantaneous positions and $\langle x_{\mathrm{PSD}} \rangle$ and $\langle y_{\mathrm{PSD}} \rangle$ are the corresponding averages.

This method is based on the notion that on average a turbulent surface is horizontal. Since the right-hand-side of equations (1) depends non-linearly on δx and δy, a zero average of $\partial h/\partial x$ and $\partial h/\partial y$ is not the same as a zero average of δx and δy, but we found the error to be negligible. Calibration requires a measurement of the height H and the conversion of measured PSD voltages to position, which was calibrated in a separate experiment. All other information needed to convert measured voltages to surface slopes follow from the measured time series. This method is straightforward, sensitive, and linear. However, it only provides the time-dependence of the surface slope in a point. For a surface that is advected by the mean flow, this information is ambiguous as temporal fluctuations may also be caused by spatial fluctuations which are swept past the measurement location. We will next describe the extension of this technique to measurement of the time-dependent gradient field along a line.

2.2 Line measurement of the surface gradient

The setup is sketched in Fig. 1b. Instead of being aimed at a single point of the surface, the laser beam is now swiveled back and forth by a rapidly oscillating mirror (an Electro Optical Products Corp. SC-30 resonant scanning mirror). Changes in the signal that occur more rapidly than those due to the oscillating motion are interpreted as spatial variations of the surface slope along the line. A drawback of this technique compared to image-based surface slope measurements is that it only provides one spatial coordinate. However, it does offer a much higher resolution in time as well as a higher spatial resolution along the line and it does not suffer from imaging ambiguities. Obviously, it is impossible to measure structures on the surface that are smaller than the size of the light spot on the surface, which is why the laser beam is passed through a lens that focuses it on the surface. As will be explained in more detail shortly, the length of the line on the surface is too large to allow the refracted beam to be projected directly onto the PSD. Hence, after passing through the free surface, the refracted beam falls onto a plate of high quality frosted glass. This leads to an illuminated dot being visible on the top side of the frosted glass, at the location where the beam hits it. This spot is projected onto the PSD. By sampling the PSD signals at a higher rate f_{s} than the oscillation frequency f_{m} of the mirror, the position of the spot on the PSD is measured multiple times during each mirror period, thereby providing the slope in multiple points on the line. In our case we can measure the slope in 152 points along a 5 cm line.

2.3 Synchronization

The electronics that control the oscillating mirror also provide a periodic square wave voltage, at the frequency at which the mirror oscillates. This signal serves as a triggering signal for a purpose-built electronic timing unit, which in turn delivers a predetermined number n of trigger signals at a fixed frequency to the ADC. This means that the positions on the line at which the PSD voltages are sampled are fixed in time relative to the phase of the mirror. This is illustrated in Fig. 2. Let us call p, $p = 1,...,n$ the index of a sample in each block of n samples and q, $q = 1,2,...$ the index of a block. Then the index p corresponds to a point on the scanned line, while the index q corresponds to the time stamp, $t_q = q / f_{\mathrm{m}}$, of the line. We will now show how the samples define the surface gradient $h_x(x,y,t)$ and $h_y(x,y,t)$.

Let us assume that the laser beam is scanned in the x-direction. The signal of the PSD contains two components: V^x and V^y corresponding to the deflections of the laser beam in the x- and y-directions, respectively. The samples $V^x_{p,q}$ include two contributions: a large harmonic contribution due to the beam being swiveled back and forth by the oscillating mirror and a smaller contribution resulting from the actual changes in slope in the points of the line. The other sampled voltage, $V^y_{p,q}$, only contains a contribution from the changes in slope.[1] Provided that the imaging by this system is linear, the position $x^g_{p,q}$ of the spot on the glass and the voltage $V^x_{p,q}$ from the PSD are related through:

$$V^x_{p,q} = A x^g_{q,p} + B^x,$$

in which A is a proportionality constant that is the same for deflections in x- and y directions and B^x is an offset that depends on the component of the measured deflection. These constants can be easily found from the measurement. Since on average the surface is flat, the time- $(q -)$ average of the measured voltage V^x is

$$V^x_p = \langle V^x_{p,q} \rangle_q = A x^g_p + B^x, \quad (3)$$

[1] In practice one can expect there to be some misalignment, leading to a small contribution due to the scanning also being present in V^y. However, this has no effect on the measurement of the slope itself, since the average trace of the spot in the surface is subtracted, as will be explained later.

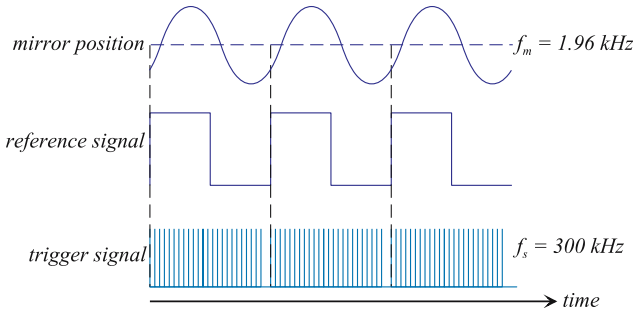

Fig. 2 Synchronization of the surface gradient scanner. The mirror control unit provides a block signal with the same frequency as the mirror movement (f_m = 1.96 kHz). This triggers a timing unit which sends blocks of 152 trigger signals at sample frequency f_s = 300 kHz to the ADC. Each line sample is one cycle of the mirror, in which each point on the line is visited twice. The unit has further provisions to synchronize the line scan to a particle image velocimetry system

where x_p^g are the time-averaged positions, $x_p^g = \langle x_{p,q}^g \rangle_q$, corresponding to the trace of the line on the glass if the surface were flat. Thus the peak-to-peak amplitude V_a^x of V_p^x corresponds to the length of the line on the glass. The proportionality constant A in Eq. 3 now follows from dividing the peak-to-peak amplitude V_a^x by the actual physical length of the line on the glass, L_g, $A = V_a^x / L_g$. Of course, since the relation between the surface slope and the laser beam deflection is non-linear, this procedure is not strictly correct. However, we have ascertained that, similar to the point measurements, the error is negligible. The constants that determine the coordinates (x_p^w, y_p^w) on the actual water surface are determined analogously to those on the glass; for example the corresponding proportionality constant would be V_a^x/L_s, in which L_s is the length of the line on the water surface.

Finally, the equations for the measured surface gradient field are similar to those of the point measurement, Eqs. 1

$$\left.\frac{\partial h(x,y,t)}{\partial x}\right|_{x=x_p^w, y=y_p^w, t=q/f_m} = \frac{\delta x_{p,q}}{n_w \sqrt{H^2 + (\delta x_{p,q})^2 + (\delta y_{p,q})^2} - H} \tag{4}$$

and similarly for $\partial h(x,y,t)/\partial y$. In Eq. 4, H is the height of the glass above the undisturbed surface and $\delta x_{p,q}$ and $\delta y_{p,q}$ are displacements of the spot on the glass with respect to the traced averaged curve:

$$\delta x_{p,q} = x_{p,q} - x_p = \left(V_{p,q}^x - V_p^x\right)/A, \tag{5}$$

and similarly for $\delta y_{p,q}$. Obviously, for a correct assignment of the gradient field it is crucial to carefully keep track of the various signs of displacements and digitized voltages.

Calibration of the line measurement of the slope is simpler than that of the point measurement as one length scale follows from the extent of the sweep. Then, calibration only needs three measured parameters: the height H of the glass above the surface, the length of the scan-line L_g on the glass, while the length of the line on the surface L_s is required in order to calculate the actual position of each point on the line on the water surface.

It should be noted that the swiveling beam crosses both the bottom of the channel as well as the surface at a small angle. The effect of this is almost completely removed by subtracting the averages (Eq. 5). Its residual effect is a small bias, which becomes somewhat more pronounced for the extreme points on the line. It is possible to correct for this, but we found the correction to be negligible. The exact position where the light beam falls onto the frosted glass depends on the slope at the surface as well as on the elevation of the surface. However, in our set-up changes of the position on the glass relative to the average position are interpreted as resulting from a change of the slope at the surface. As with the point measurements, the influence of changes in the elevation of the surface is neglected, since their effect is very small compared to the effect of a change in the slope, especially since the anticipated changes in the elevation (at most a few mm) are tiny compared to H (30 cm).

The use of a plate of frosted glass is an unfortunate necessity. The reason is that the optics needed to directly project the refracted laser beam onto the PSD is subject to incompatible requirements. Let us briefly discuss such direct imaging using a lens between the surface and the detector. The optimal placement of the detector is in the focal plane of the lens. Then, the displacement signal is only determined by the deflection angle of the laser beam, and thus by the surface gradient. Let S_m be the largest gradient which should be measured; in our experiments $S_m = \mathcal{O}(0.3)$. The focal length F of the lens is then determined by $S_m = d/F$, where d is the diameter of the detector. For the used detector with d = 2 cm, this gives $F \approx 7$ cm. The minimum diameter of such a lens is the same as the length L_s = 5 cm of the scan line. Lenses that have focal lengths that are of the same order as their diameter are hard to come by. Little would be gained by positioning the detector short of the focal length of the lens as it increases the required lens diameter. The problem is that in direct imaging of the refracted laser beam, angle and position are coupled.

The only solution is to break this connection by using a frosted glass screen. A drawback of this method is, however, a large loss of light intensity and the introduction of speckles in the light spot. To optimize the light intensity the laser spot on the frosted glass is imaged onto the PSD detector surface by using two very strong large-diameter lenses. To further increase the intensity of the light on the PSD a relatively powerful (approx. 30 mW) He–Ne laser was used.

The time response of the PSD itself now determines the signal-to-noise ratio in our scan technique. Since the position signal of the light spot depends on intensity ratios, the position signal is insensitive to intensity fluctuations of the refracted laser beam. In our experiment, intensity fluctuations are caused by scattering off particles in the flow (used in PIV experiments) and by speckles of the frosted glass screen. However, the intensity normalization can only work if all currents are measured simultaneously. The problem is that photocharges in the PSD have a finite velocity, set by the capacity of the light-sensitive layer. The propagation delay is a few μs, which in our case corresponds to the used sampling frequency (f_s = 300 kHz). At those frequencies intensity variations are seen as position variations. Without a faster PSD, no further improvement of the signal-to-noise ratio is possible. The positions x^p on the scan line are sampled sinusoidally: the points crowd near the extremes of the sweep, and they are sampled fastest near the zero crossings of the sweep. We expect that a further effect of the propagation delays of the photo-charges is that samples of the surface slope near the zero crossings will have different properties from those at the extremes of x_p. We will assess this possible source of inhomogeneity below.

3 Data processing

The data processing is done with a series of computer programs. In order to obtain surface gradient information from the stored data, the file (typically several GBytes in size) is first unravelled in samples $V^x_{p,q}$ and $V^y_{p,q}$. If, for example, the laser beam is scanned in the x-direction sample $V^x_{p,q}$ contains the relevant information about the scan. Since perfect synchronization is crucial for this method, the relative phase of the samples $V^x_{p,q}$ is monitored constantly through forming the correlation $\langle V^x{}_{p,q} \sin(2\pi p f_m/f_s)\rangle$. Phase drifts may occur due to temperature changes of the resonant mirror. Our measurement of the phase reveals that the relative phase-shift of the mirror is $\mathcal{O}(10^{-3})$ over the duration of the longest measurement, which is negligible. Next, the coordinates (x_p,y_p), $p = 1,...,n$ are computed from phase-sensitive averages of V^x and V^y. Finally the surface gradients $h_x(x_p,y_p,t_q)$ and $h_y(x_p,y_p,t_q)$ are computed.

The key questions are about the homogeneity of the measurement technique along the scan line and its spectral response. Several useful statistical quantities can be computed from the measured gradient field and may be used to answer these questions. In the case of homogeneous turbulence, the normalized space–time correlation function

$$R^{xx}(x_i,x_j,\tau) = \frac{\langle h_x(x_i,t+\tau)h_x(x_j,t)\rangle}{\langle h_x^2(x_i,t)\rangle^{1/2}\langle h_x^2(x_j,t)\rangle^{1/2}} \tag{6}$$

and similarly R^{yy}, R^{xy}, depends only on the separation $r = x_i - x_j$, and not on the individual coordinates x_i, x_j. As different points x_i on the scan line are traversed with different velocities of the swiveling laser beam, the question is whether this property holds for the measured correlation function. We approach the correlation function through the cross-spectral density

$$\widetilde{C}^{xx}(x_i,x_j,\omega) = \left\langle \widetilde{h}_x(x_i,\omega)\widetilde{h}^*_x(x_j,\omega)\right\rangle.$$

where $\tilde{h}_x$ is the temporal Fourier transform of h_x. The advantage of the cross-spectral density is that it involves Fourier transforms in the homogeneous time direction, but it retains the dependence on the spatial coordinates. In order to improve the statistical accuracy of $\widetilde{C}^{xx}$ we perform a frequency average

$$\int K(\omega,\omega')\widetilde{C}^{xx}(x_i,x_j,\omega')\mathrm{d}\omega',$$

where the kernel $K(\omega, \omega')$ is a tent-function centered on ω, and whose width in ω' increases exponentially with increasing ω. Such an average is most appropriate for energy spectra that have an algebraic dependence on the frequency. From the cross-spectral density we can compute the frequency spectrum at each spatial point, $E_{xx}(x_i,\omega) = \widetilde{C}^{xx}(x_i,x_i,\omega)$. Finally, the covariance function Eq. 6 is only a Fourier transform away

$$R^{xx}(x_i,x_j,\tau) = \frac{\Re\int_0^\infty \mathrm{e}^{\mathrm{i}\omega\tau}\widetilde{C}^{xx}(x_i,x_i,\omega)\mathrm{d}\omega}{\left(\int_0^\infty \cos(\omega\tau)\widetilde{C}^{xx}(x_i,x_i,\omega)\mathrm{d}\omega\ \int_0^\infty \cos(\omega\tau)\widetilde{C}^{xx}(x_j,x_j,\omega)\mathrm{d}\omega\right)^{1/2}}, \tag{7}$$

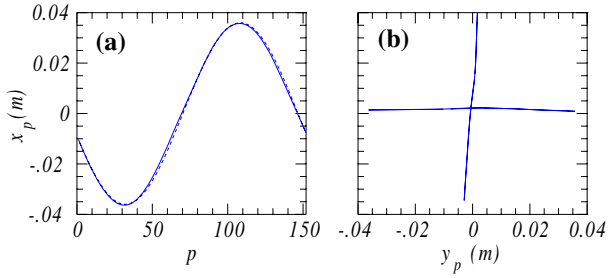

Fig. 3 Linearity of the imaging by the surface scan set-up. **a** A harmonic scan in streamwise direction. *Full line* the average coordinate y_p^w computed for a turbulent surface. Because of the harmonic scan, y_p^w should ideally be $\propto \sin(2\pi p f_m / f_s + \phi)$. *Dashed line A* $\sin(2\pi p f_m / f_s + \phi)$, with amplitude A set to the amplitude of y_p^w and measured phase $\phi = 1.088\ \pi$

where $\Re$ denotes the real part. We will demonstrate that to good approximation the covariance function R only depends on the separation of the points, and not on their individual coordinates.

$$r_k = x_i - x_j,\ k = 1, \ldots, n(n-1)/2.$$

However, significant errors do exist. Clearly, computing the space–time correlation function of the surface gradient by means of the cross-spectral density is the only practical option, as direct computation in the time domain would take prohibitively long.

Direct computation of the spectrum of the surface gradient, $\tilde{h}(k_x, \omega)$, is possible by resampling the coordinates along the line, x_p in our example, and then performing a fast-Fourier transform both in space and time. The surface fields $h_x(x,y,t)$ and $h_y(x,y,t)$ themselves are stored for further processing, for example in order to assess the validity of Taylor's frozen turbulence hypothesis for the surface. Although we only have information about a single spatial dimension (and time), the gradient field signals allow us to measure statistical quantities of a turbulent surface which, to our knowledge, have not been measured before.

4 Results

Before proceeding with the experimental results for the surface above grid-generated turbulence as well as a first physical interpretation, we will first take a look at a number of tests of the surface scan technique. We need to test wether the imaging of the scan line through the frosted glass, the lenses and the PSD is linear, since this is one of the assumptions made in the previous section. Further tests revolve around the frequency response of the PSD. The PSD needs to be able to follow changes in the position of the spot on its surface faster than the mirror frequency (approximately 2 kHz), since these are to be interpreted as spatial variations. Our first interest will be the average positions x_p^w and y_p^w.

The oscillating mirror swivels the laser beam approximately harmonically in time. Hence, for a scan line in x-direction the average position of the spot on the PSD surface should depend on p as $\sin(2\pi p / f_s + \phi)$. This is very nearly so, as is illustrated in Fig. 3a. We conclude that non-linearity effects in the imaging are small.[2] Figure 3b shows x_p versus y_p, i.e. the trace of the surface scan for both a spanwise and streamwise scan. This figure shows that the adjacent points in a scan form an approximately straight line, as intended. Furthermore, Fig. 3b shows that the PSD and its associated electronics can follow the illuminated spot on the surface, even though it moves back and forth at almost 2 kHz. Any phase difference between the measured x- and y-deflections would have resulted in a Lissajous-loop.

The alignment of the set-up is relatively straightforward. The hardest part is aligning the direction of the scan line. Changing the direction of the scan line, which is very useful when studying the isotropy of the surface gradient field, involves moving the oscillating mirror, the focusing lens, and several mirrors. Yet, it is possible to properly align the scan-line in spanwise direction as well as aligning it in a practically perpendicular, i.e. in streamwise, direction, at essentially the same location in the channel. This can also be seen from Fig. 3b.

A first impression of the detector homogeneity can be obtained from the probability distribution function (PDF) of surface gradients on a turbulent channel flow. The variation of the PDF along the scanned line is shown in Fig. 4. In this experiment, the scanned line points in the x-direction. As the length L_s of the scanned line is 5 cm, which is much smaller than the width of the channel (30 cm), we can assume that the turbulence is homogeneous. The measured PDF is very nearly independent of the position on the scanning line, but a small systematic effect for the rare large $|dh/dx|$ events can be seen. Figure 4 also demonstrates that the gradient fluctuations are very nearly Gaussian. A quite similar result was obtained for scans in the streamwise (y) direction. In this direction the grid-generated turbulence decays, but the variation of its statistical properties over the length of the scan line is

[2] The quality of the harmonic fit is not only due to the linearity of the imaging. Deviations of the harmonic dependence and curved scan lines can also occur due to the axis of rotation of the mirror not being parallel to the mirror surface.

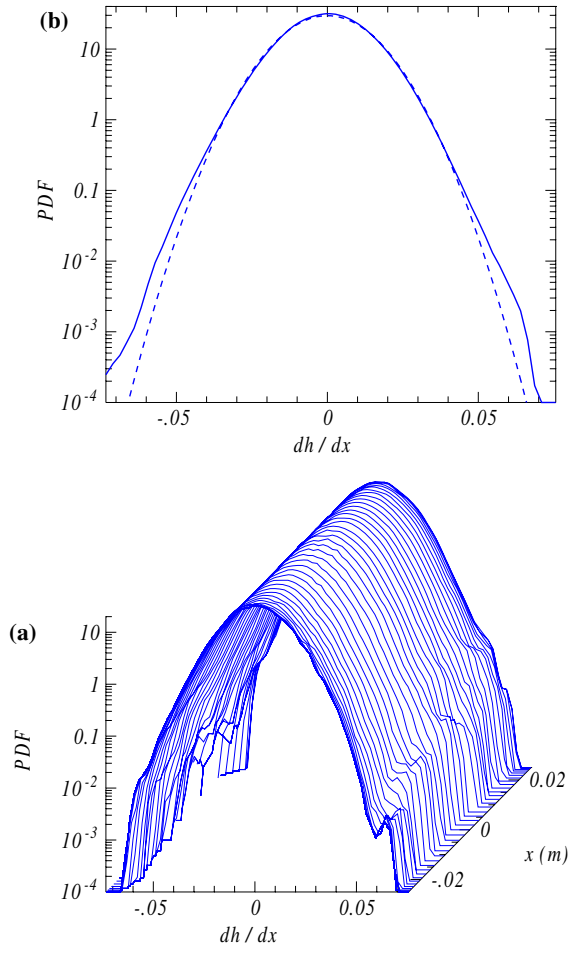

Fig. 4 **a** Probability density function (PDF) of surface gradients dh/dx as a function of the position x on the scan line. The *scan line* is oriented perpendicularly to the mean flow velocity in the channel. **b** *Full line* PDF averaged over x *dashed line* Gaussian fit. The turbulence with mean velocity U = 0.25 m/s is generated with an active grid

negligible as L_s = 5 cm is small compared to the distance (2 m) of the scanner behind the turbulence generating grid.

In order to see how scanning affects the signal-to-noise ratio, we will now compare frequency spectra of the surface slope in a point measured with the surface scanning technique to spectra measured under the same experimental conditions but with a point-measurement. In the last case, the surface slope follows directly from the registered signal, while it is wrapped in the spatial scan in the first case.

The frequency spectrum obtained from the line scan in this case is actually the frequency spectrum in one of the 152 points on the 5 cm long line. Results obtained with both techniques for static grid generated turbulence, are shown in Fig. 5a. Up to a frequency of 50 Hz the spectra are very similar, despite the different PSD signal processing electronics, different PSDs, the very different optical systems as well as the difference in calibration methods. Above 50 Hz the spectra from the scan are drowned in noise, while the point spectra continue up to roughly 1 kHz. This is not due to a limitation in frequency response, however, since we have already seen that the PSD and its electronics can follow the spot moving back and forth at almost 2 kHz. The difference between the spectra is due to the lower signal-to-noise ratio as a result of the spot's relatively low-light intensity, and the presence of the ground glass screen. Still, the spectrum from the scan covers several orders of magnitude.

The frequency spectrum of the slope in a point on a surface scan line should be completely independent from the direction of that line. However, such a dependence may be found if the slope measurement is affected by the scan speed as the light spot moves far quicker in the scan-direction than perpendicular to it. A comparison of spectra measured in a spanwise scan with those measured with the scan line in the streamwise direction can potentially reveal limitations in the detector's frequency response. In Fig. 6 we show slope energy spectra E_{xx} and E_{yy} obtained from measurements along both a streamwise and spanwise line, averaged over the line, for active grid generated turbulence. Indeed the frequency spectrum of either slope is practically independent of the direction of the scan line, demonstrating that the registered signals can be unravelled adequately in position and slope information.

The next concern is the frequency-dependent homogeneity of our surface scan detector. Figure 7 shows the dependence of measured frequency spectra on the position on the scan line. The fluctuations appear slightly depressed in the center of the scan line, in a way that does not depend on frequency. Most probably, this reduction of the sensitivity is related to the variation of the scan speed, which is largest in the center, in combination with the speckle patterns of the ground glass screen. This effect can be eliminated adequately by normalizing measured wave slopes by their root mean square values $\langle h_x^2 \rangle^{1/2}$ and $\langle h_y^2 \rangle^{1/2}$.

Let us finally turn to the spatial correlation function $R(x_i,x_j,\tau)$ at τ = 0. In Fig. 8 we plot $R^{xx}(r_k,\tau)$ and $R^{yy}(r_k,\tau)$, where r_k is the separation $r_k = x_i - x_j$, k = 1, 2, ..., 11476 and τ = 0. Clearly the correlation function is not just a function of the separation, but also of the individual coordinates x_i, x_j. The resulting deterministic noise is determined by the different scan speeds with which the laser beam passes different points on the scan line. It affects measured spatial spectra at high wavenumbers. In the correlation functions shown later,

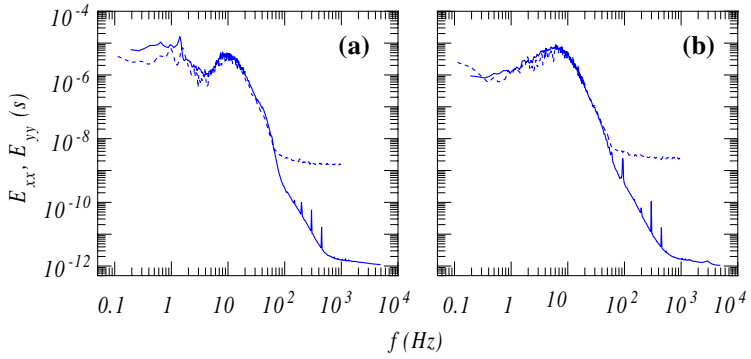

Fig. 5 Comparison of frequency spectra of the slope measured with point-measurements and derived from line measurements. The turbulence with mean-stream velocity of $U = 0.28$ m/s was generated with a static grid. **a** E_{yy}, point spectra of the streamwise slope. **b** E_{xx}, point spectra of the spanwise slope. *Full lines* using a point measurement, *dashed lines* spectra in one of the points of a line measurement

this effect was cured by fitting a 6th order polynomial to their r-dependence.

Scanning techniques are unavoidable for measuring the surface gradient field. The challenge is to unravel gradient- from position information. Its success is determined by the optics and by the response time of the position detector, both of which compromise the signal-to-noise ratio. Clearly, the scan frequency should be adapted to the problem at hand. Currently, $f_m = 1.96$ kHz, but judging from Fig. 5, a reduction to 1 kHz would be possible, resulting in an improvement of the signal-to-noise ratio.

5 Taylor's hypothesis of a turbulent surface

In turbulent flows with a relatively large mean flow, Taylor's hypothesis can be invoked to turn time-dependent measurements in a stationary point to space-dependent measurements. The idea is that turbulent fluctuations remain frozen while they are advected by the mean flow. In measurements of the turbulent velocity field with moderate turbulence intensity, $u/U \lessapprox 0.1$, Taylor's hypothesis works well (Gledzer 1997). The question now is whether Taylor's hypothesis also applies to the free surface of a turbulent flow, that is whether we can interpret spanwise line scans as 2D *spatial* scans of the surface. Using this hypothesis, we would be able to construct surfaces from measured $h_{x,y}(x, t)$ as $h_{x,y}(x, y) = h_{x,y}(x, U\,t)$, with U the mean velocity. Clearly, Taylor's hypothesis does not hold if the turbulent surface changes rapidly while it is advected through the scanning line by the mean velocity.

In order to assess the applicability of Taylor's hypothesis to a turbulent surface, we will reconstruct surfaces from time-dependent line measurements, and test whether these reconstructed surfaces, like as the true surface, are potential. For a potential surface the circulation of the gradient field taken around a loop of size r,

$$\Gamma_r = \oint_S \nabla h(x,y)\mathrm{d}\mathbf{s}$$

vanishes for any loop S. We have computed Γ_r for our reconstructed turbulent surfaces; for the loops we chose squares with size r. Since the sides in the y-direction of these squares are derived from the

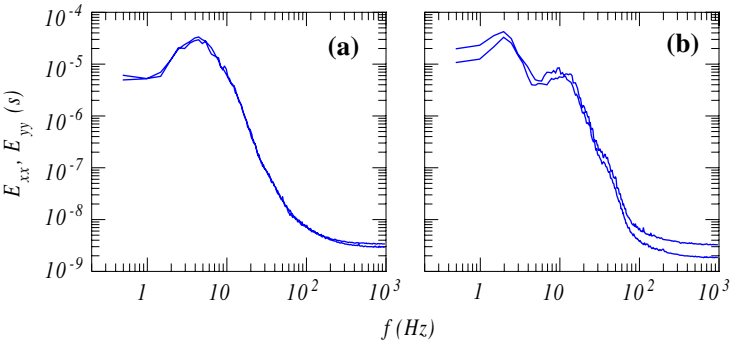

Fig. 6 **a** Point spectrum of the spanwise slope, E_{xx}, from both a spanwise and streamwise scan. **b** Point spectrum of the streamwise slope, E_{yy}, from both a spanwise and streamwise scan. The turbulence with mean velocity $U = 0.25$ m/s was generated using an active grid

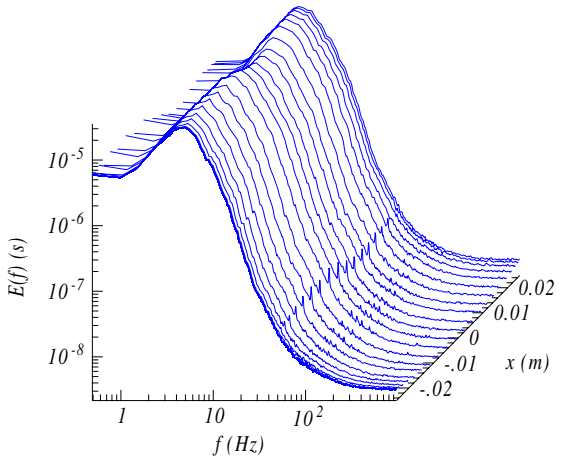

Fig. 7 Point frequency spectra as a function of the position of the point x on the scan line. The depression in the center of the scan line signifies a reduction of the gradient-detector sensitivity. Since it equally affects all frequencies, it can be cured by normalizing the signals with their rms value

temporal dependence of the scan lines, Γ_r will be non-zero if the surface is not frozen, and Taylor's hypothesis does not apply. Because Γ_r is a fluctuating quantity with mean zero, we take

$$\delta h_0(r) = \left\langle \Gamma_r^2 \right\rangle^{1/2}$$

as a measure for the error, which can be viewed as an error in the elevation of the surface measured over a distance r. Registered time series of line measurements were tiled in non-overlapping reconstructed 2D surfaces, and the average was done both over all surfaces and over the area of each surface. We can compare $\delta h_0(r)$ to the rms surface elevation

$$\delta h_x(r) = \left\langle \left(\int_r h_x(x) \mathrm{d}x \right)^2 \right\rangle^{1/2},$$

which is measured in the scan direction and is not affected by the frozen turbulence hypothesis. In Fig. 9 we show both $\delta h_0(r)$ and $\delta h_x(r)$ as a function of r. Both quantities increase algebraically; as expected $\delta h_0(r)$ increases more quickly than $\delta h_x(r)$ as it embodies the temporal fluctuations of the surface.

Figure 9 clearly demonstrates that Taylor's frozen turbulence hypothesis does not hold for a free surface above a turbulent flow. On one hand, this is quite remarkable as it works well for the turbulent velocity field beneath it. On the other hand, the turbulent velocity field excites capillary-gravity waves on the surface. As is well known, for water the minimum phase velocity of capillary-gravity waves is approximately 0.2 m/s, which is comparable to the mean flow velocity in our experiments.

The breakdown of the frozen turbulence hypothesis is further illustrated in Fig. 10 where we show the space–time correlation function $R^{yy}(y, \tau)$ measured in a

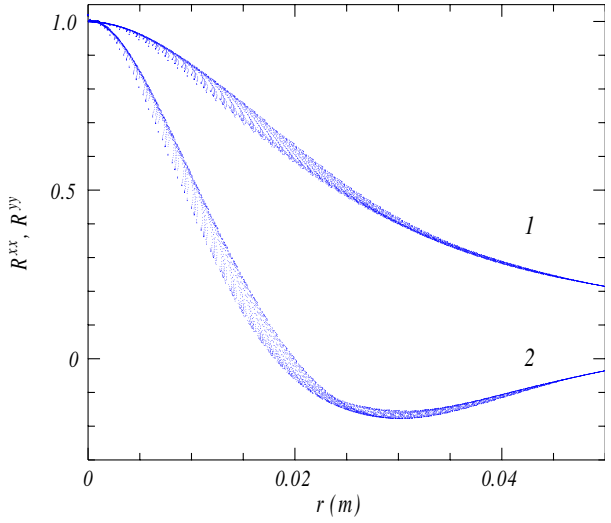

Fig. 8 Longitudinal (*1*) and transverse (*2*) spatial correlation functions measured along a streamwise line as a function of the separation $r_k = x_i - x_j$. We draw as many points r_k as there are separations between x_i, $i = 1,...,152$ on the scan line. The residual dependence on the individual coordinates x_i shows as deterministic noise

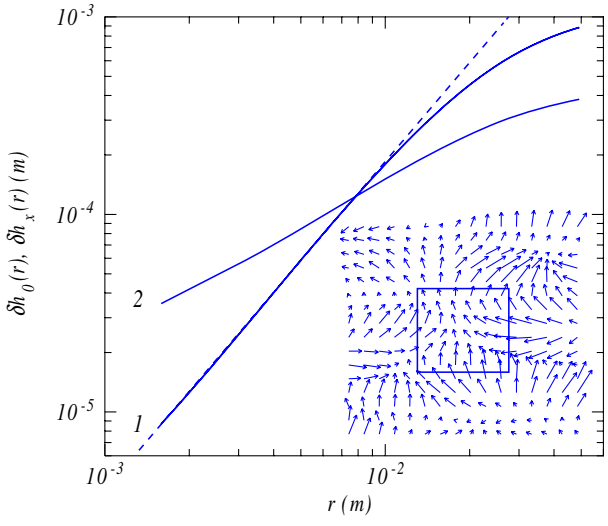

Fig. 9 Error made when assuming Taylor's frozen turbulence hypothesis for turbulent surfaces. (*1*) *Full line* root mean square circulation $\delta h_0(r)$, *dashed line* $\delta h_0(r) \sim r^{1.7}$. (*2*) Root mean square elevation $\delta h_x(r)$ measured along the scan line. The inset shows the vector field $\nabla h(x, y)$ which was constructed using the frozen turbulence hypothesis. The error is quantified by the value of the circulation of $\nabla h(x, y)$ taken around squares with size r. The turbulence with mean velocity $U = 0.25$ m/s was generated using an active grid

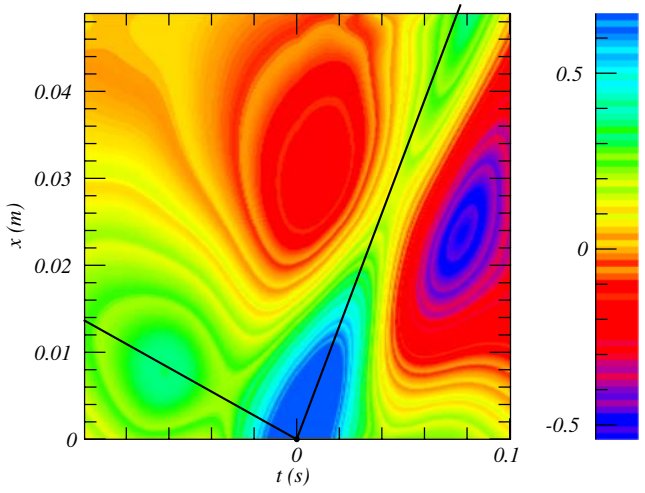

Fig. 10 Space–time correlation function of a turbulent line measurement, scanned in the streamwise (y)-direction. *Full lines* structures traveling with $v = 0.14$ m/s and $v = -0.64$ m/s corresponding to the ridges in the correlation function The turbulence with mean velocity $U = 0.25$ m/s was generated using an active grid

streamwise scan of the turbulent surface. If indeed Taylor's hypothesis would hold, the correlation function would reduce to the ridge $R^{yy} = \delta(y - \tau U)$, with U the mean velocity. This is clearly not the case. Instead, two ridges can be discriminated, *not* at the mean velocity, but at velocities $U \pm v_f$, with $v_f = 0.40$ m/s. It is tempting to associate the velocity v_f with the phase velocity of capillary-gravity waves with wavelength $\lambda = 0.1$ m. It turns out that this wavelength is close to the integral scale of the turbulent velocity field. We conclude that violation of the frozen turbulence hypothesis of turbulent surfaces is related to the emergence of capillary-gravity waves.

6 Conclusions

Characterizing a turbulent surface through refraction of a focused laser beam is precise, linear and, since the signal depends on the surface gradient, can resolve large surface wavenumbers. However, using this technique to obtain space–time information presents a challenge. In this paper, we describe a scanning method in which a laser beam is rapidly scanned over a surface and its position after refraction is measured synchronously. The synchronization problem can be solved readily, but this method challenges the speed of current position sensing detectors. Further, imaging requirements necessitated the use of a translucent screen, resulting in a deterioration of the signal-to-noise ratio. The result is a device that can measure the space–time gradient field of a turbulent free surface with good precision.

The resolution in space is set by the size of the focus of the laser beam (≈ 0.3 mm), whereas in principle the resolution in time is half the swiveling frequency f_m of the mirror ($f_m/2 \approx 1$ kHz). However, for our very steep spectra of the surface slope above turbulence the noise threshold is reached at 100 Hz. The alignment of the scanning set-up is straightforward and it requires no calibration other than a measurement of a few lengths. In principle, the technique can easily be adapted for measuring reflection instead of refraction. By using lasers with different wavelengths and separating the images using laser line filters, this technique can be easily combined with other optical diagnostics, such as particle image velocimetry, as was actually done in our experiments.

We have discussed a number of statistical quantities that can be measured from space–time signals. Although a complete discussion of the meaning of these quantities falls outside the scope of this paper, we demonstrate that spectra and correlation functions can be measured precisely. We have also found that Taylor's frozen turbulence hypothesis, applicable to the measurement of the turbulent velocity field with a relatively large mean velocity, does not hold for its turbulent free surface due to the emergence of relatively fast capillary-gravity waves.

Acknowledgments This work is part of the research programme of the 'Stichting voor Fundamenteel Onderzoek der Materie (FOM)', which is financially supported by the 'Nederlandse Organisatie voor Wetenschappelijk Onderzoek (NWO)'.

References

Bock E, Hara T (1995) Optical measurements of capillary gravity waves using a scanning laser slope gauge. J Atmos Ocean Technol 12:395–403

Cox C, Munk W (1954) Statistics of the sea surface derived from sun glitter. J Marine Res 16:199–225

Dalziel S, Hughes G, Sutherland B (2000) Whole-field density measurements by 'synthetic schlieren'. Exp Fluids 28:322–335

Dugan J, Piotrowski C (2003) Surface current measurements using airborne visible image time series. Remote Sens Environ 84:309–319

Forbes C, Leman K, Olson D, Brown O (1993) Eddy and wave dynamics in the south atlantic as diagnosed from geosat altimeter data. J Geophys Res 12:297–314

Gharib M (1994) Some aspects of near surface vortices. Appl Mech Rev 47:S157–S162

Gharib M, Weigand A (1996) Experimental studies of vortex disconnection and surface connection at a free surface. J Fluid Mech 321:59–86

Gledzer E (1997) On the Taylor hypothesis corrections for measured energy spectra of turbulence. Physica D 104(2):163–183

Hara T, Bock E, Donelan M (1997) Frequency-wavenumber spectrum of wind-generated gravity-capillary waves. J Geophys Res 102:1061–1072

Holland T (2001) Application of the linear dispersion relation with respect to depth inversion and remotely sensed imagery. IEEE Trans Geosci Remote Sens 39:2060–2072

Jähne B, Klinks J, Waas S (1994) Imaging of short ocean wind waves: a critical theoretical review. J Opt Soc Am A 11(8):2197–2209

Kurata K, Grattan K, Uchiyama H, Tanaka T (1990) Water surface measurements in a shallow channel using the transmitted image of a grating. Rev Sci Instrum 6:736–739

Sarpkaya T, Suthon P (1991) Interaction of a vortex couple with a free surface. Exp Fluids 11:205–217

Senet C, Seemann J, Ziemer J (2001) The near-surface current velocity determined from images sequences of the sea surface. IEEE Trans Geosci Remote Sens 39:492–505

Settles G (2001) Schlieren and Shadowgraph techniques, visualizing phenomena in transparent media. Springer, Berlin Heidelberg New York

Stammer D (1997) Global characteristics of ocean variability from regional topex/poseidon altimeter measurements. J Phys Oceanogr 27:1743–1769

Walker D, Chen CY, Willmarth W (1995) Turbulent structure in free-surface jet flows. J Fluid Mech 291:223–261

Weigand A (1996) Simultaneous mapping of the velocity and deformation field at a free surface. Exp in Fluids 20:358–364

Westra MT, Binks DJ, van de Water W (2003) Patterns of Faraday waves. J Fluid Mech 496:1–32

Zhang X, Cox C (1994) Measuring the two-dimensional structure of a wavy water surface optically: a surface gradient detector. Exp Fluids 17:225–237